We are IntechOpen, the world's leading publisher of Open Access books Built by scientists, for scientists

6,900
Open access books available

185,000
International authors and editors

200M
Downloads

Our authors are among the

154
Countries delivered to

TOP 1%
most cited scientists

12.2%
Contributors from top 500 universities



WEB OF SCIENCE™

Selection of our books indexed in the Book Citation Index in Web of Science™ Core Collection (BKCI)

Interested in publishing with us?
Contact book.department@intechopen.com

Numbers displayed above are based on latest data collected.
For more information visit www.intechopen.com



Chapter 3

Membrane Separation Technology in Carbon Capture

Guozhao Ji and Ming Zhao

Additional information is available at the end of the chapter

http://dx.doi.org/10.5772/65723

Abstract

This chapter introduces the basics of membrane technology and the application of membrane separation in carbon capture processes. A number of membranes applicable in pre-combustion, post-combustion or oxy-fuel combustion have been discussed. An economic comparison between conventional amine-based absorption and membrane separation demonstrates the great potential in membrane technology.

Keywords: membrane separation, carbon dioxide capture, pre-combustion, post-combustion, oxy-fuel combustion

1. Introduction

Gas separation by membrane is attractive in low carbon emission technologies, as it can be operated in a continuous system, which is preferred by industry, other than the conventional batch systems such as adsorption and absorption. Feeding of mixed gas and exiting of purified gas can happen at the same time. Membrane selectively permeates the desired components and retains the unwanted, resulting in separation of gas mixtures. In carbon capture and storage (CCS) processes, CO_2 has to be separated from the exhaust gas streams before the subsequent transportation and storage. Membrane separation technology is one of efficient solutions for carbon capture.

There have been a number of books regarding membrane technology. However, most of them are about liquid separation and very few are found for CCS. This chapter aims at introducing and demonstrating the membrane technology in CCS. The application of membrane in carbon capture mainly includes H_2/CO_2 separation for pre-combustion, CO_2/N_2 separation for post-combustion and O_2/N_2 separation (air separation) for oxy-fuel combustion. There is a wide variety of membrane types based on its physical and chemical property. Many of them have showed great potentials to fulfill the need of CCS.

INTECH
open science | open minds

© 2017 The Author(s). Licensee InTech. This chapter is distributed under the terms of the Creative Commons Attribution License (http://creativecommons.org/licenses/by/3.0), which permits unrestricted use, distribution, and reproduction in any medium, provided the original work is properly cited. CC BY

2. Overview of membranes

Membrane performs as a filter. It allows certain molecules to permeate through, while blocks other specific molecules from entering the membrane as demonstrated in **Figure 1**. Membrane has already been widely used in liquid separations such as micro-filtration, ultra-filtration, reverse osmosis, forward osmosis, desalination and medical application. However, gas separation using membrane is still developing. Membrane gas separation has attracted intensive researches in CCS field during recent years.

Gas permeation flux across unit membrane area under unit pressure difference through unit membrane thickness is called permeability (mol s^{-1} m^{-2} Pa^{-1}) and the ratio of permeabilities of different gases through the same membrane is defined as selectivity. The gas separation mechanism varies from membrane to membrane. The selectivity of different gases may result from the difference in molecular size, affinity to membrane material, molecular weight, etc., depending on the gas and membrane of interest.

In order to achieve high permeate flux, the feed gas is pressurized, while the permeate gas is connected to atmosphere or vacuum to obtain a higher driving force. However, since the thickness of a membrane is only several hundred nanometers to several microns, it is impossible to resist this force. So a membrane is normally coated onto a thick, porous substrate to achieve enough mechanical strength. The supporting substrate should offer minimum flow resistance, thus containing large pores, which allows free flow of gas that has permeated the top layer. In case of too large pores and highly rough surface on the substrate, membrane defects such as cracking and peeling may occur. An interlayer with much smaller pore size (than substrate pore size) can enable smoother transition in between. This design is referred to as asymmetric structure as shown in **Figure 2**.

In the current Research & Developments (R&Ds) of membrane, the most popular mechanism is size sieving separation. Therefore, the key parameter of a membrane is its pore size. By

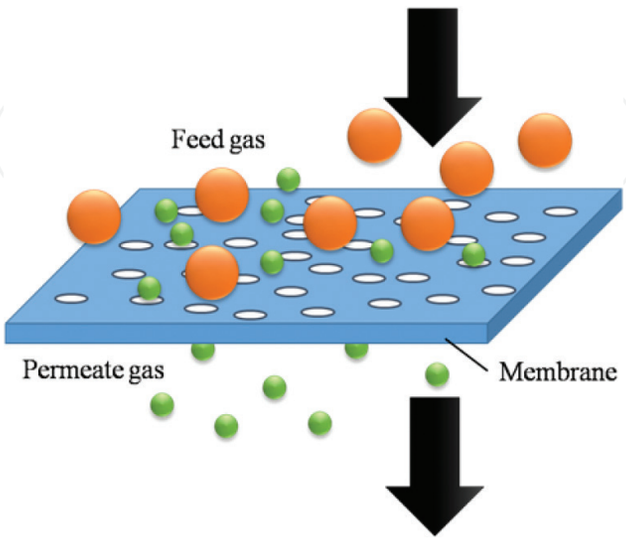


Figure 1. The schematic of membrane separation for binary gas mixtures.

http://dx.doi.org/10.5772/65723

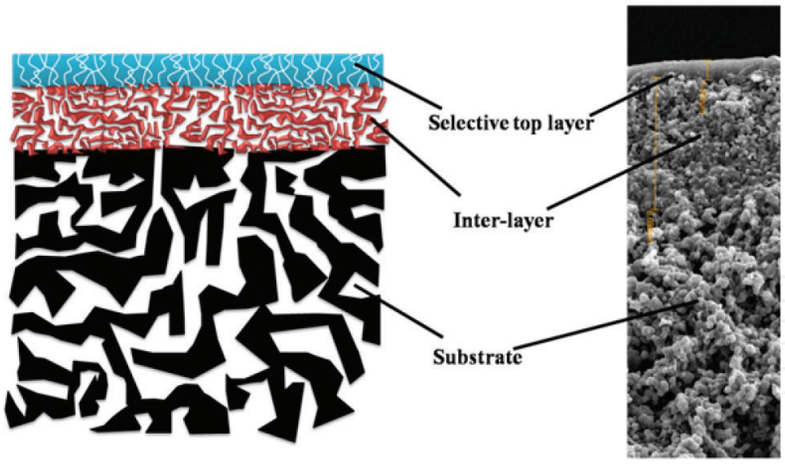


Figure 2. The asymmetric structure of membrane coated on a substrate.

pore size, membranes are classified into three categories that are listed in **Table 1**. In addition, one more type of membrane that is nonporous, therefore called dense membrane, is also discussed in this chapter.

2.1. Advantages of membranes

Compared to conventional CO_2 removal technologies, membrane has shown great potential in CCS owing to its characteristics listed below:

Low capital cost

Membrane requires little material to coat. It does not need additional facilities such as large pretreatment vessel and solvent storage.

Low operating cost

The main operating cost for membrane separation unit is only membrane replacement. Due to the smaller size and weight of membrane, the cost is much lower than the conventional techniques, which replace the large amount of solvent or sorbent.

Simplicity and reliability

Since membrane does not show fast decay in performance that most likely occurs to the traditional solvents or sorbents, it can be running unattended for long periods. Another character of membrane is that gas does not stay and reacts with membrane, so membrane has no saturation and thus avoids frequent shut down and start-up.

Pore classification	Pore size range (nm)
Micropore	<2
Mesopore	2–50
Macropore	>50

Table 1. Membrane classification by pore size.

Adaptability

Membrane system is designed and operated to remove the required percentage of CO_2 instead of the absolute quantity of CO_2 removal. Variations in the feed CO_2 concentration can be adjusted by varying the space velocity to keep constant product quality.

Design efficiency

Membrane system can integrate a number of processes into one unit, such as Hg vapor removal, H_2S removal and dehydration. Traditional CO_2 removal techniques have to operate these steps separately.

Easy for remote area

Multiple membranes could be packed into one module to reduce size and weight, which not only increases membrane area in unit volume but also makes it easier to transport to remote locations. Simple installation is feasible at which spare parts are rare, labors are unskilled and additional facilities (such as solvent storage, water supply and power generation) are short in supply.

2.2. Membrane fabrication

Membrane fabrication involves how to coat the selective layer onto the porous substrate. The fabrication process has significant influence on the membrane property such as membrane uniformity and thickness. The membrane coating technique includes dip-coating, chemical vapor deposition (CVD), spinning and spraying. Among them, the most popular and mature methods are dip-coating and CVD. This section will demonstrate these two technologies.

2.2.1. Dip-coating

Dip-coating involves dipping the macro-porous substrate in a solution and in turn, the solution is coated on the substrate, which is followed by a dehydration process at a lower temperature. It is the oldest and the simplest film deposition method. The dip-coating process can be separated into five stages: immersion, start-up, deposition, drainage and evaporation **(Figure 3**).

Immersion: The substrate is immersed in the solution of the coating material at a constant speed to avoid jitter.

Start-up: The entire substrate has remained inside the solution for a while and is starting to be pulled up.

Deposition: The thin layer of solution deposits itself on the surface of the substrate when it is pulled up. The withdrawing speed is constant to avoid any jitters. The speed determines the thickness of the coating. Faster withdrawal speed gives thicker layer and vice versa.

Drainage: Excess liquid will drain from the surface back to the solution due to the gravity.

Evaporation: The solvent evaporates from the liquid, forming the thin layer. Evaporation normally accompanies the start-up, deposition and drainage stages.

http://dx.doi.org/10.5772/65723

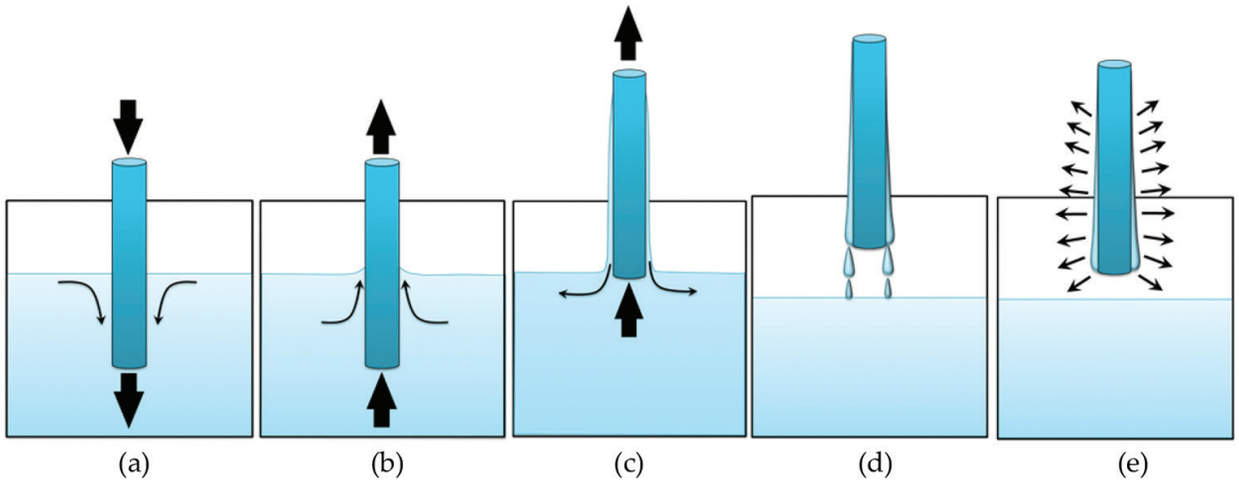


Figure 3. Dip-coating stages: (a) immersion; (b) start-up; (c) deposition; (d) drainage and (e) evaporation. Reproduced from Brinker [1].

2.2.2. Chemical vapor deposition (CVD)

Another common membrane coating technique is CVD. CVD modifies the properties of a substrate surface by depositing a thin layer of film via chemical reactions in a gaseous medium surrounding the substrate at elevated temperatures.

The process of CVD includes transporting the reactant gases and/or carrier gas into a reaction chamber, which is followed by a deposition process to form a film. The film coating could be performed by decomposition, oxidation, hydrolysis or compound formation. The reactions normally take place in the gaseous phase and the intermediate gases adsorb on the substrate followed by surface reactions. The detailed steps of CVD process are demonstrated in **Figure 4**.

1. Reactant feeding: Delivering the reactant gaseous species into the reaction chamber.
2. Reaction: Chemical reactions of the reactant gas species under heating condition to form intermediates.
3. Diffusion to substrate: Diffusion of gases through the boundary layer to the substrate surface.
4. Adsorption on the substrate: Adsorption of reactant species or intermediates on substrate surface.
5. Surface migration: Inclusion of coating atoms into the growing surface and formation of by-product species.
6. By-product desorption: Desorption of by-product species of the surface reaction.
7. By-product diffusion: Diffusion of by-product species to the bulk phase.
8. By-product exiting: Transport of by-product gaseous species away from substrate and exit the reaction chamber.

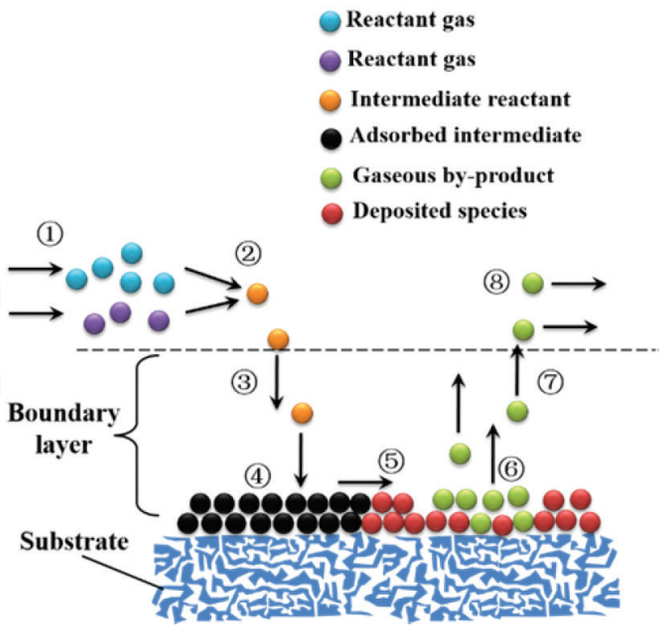


Figure 4. Schematic model of a CVD process. Reproduced from Khatib et al. [2].

As illustrated above, CVD is more complicated technique than dip-coating, thus the manufacture cost of a membrane is relatively higher than that of dip-coating. The advantage of CVD is good reproducibility over dip-coating as the latter may suffer from a lack of reproducibility.

2.3. Membrane separation mechanism

A membrane can separate gas mixture because different gases have different permeability through the membrane. The permeate flux across unit membrane area under unit pressure gradient is called permeability and the ratio between permeability of gas A and that of gas B is defined as selectivity of A to B. In order to achieve separation, a greater difference between gas permeabilities is preferred. This difference comes from their physical and/or chemical properties as well as the interaction with membrane.

2.3.1. Size sieving

The most widely known separation mechanism is size sieving. The membrane pore size is just between the smaller gas molecule and larger gas molecule as depicted in **Figure 5**. The smaller gas molecule A passes the pore channel freely, while the counterpart gas B is not able to enter the pore. As a result, pure component A is obtained in the permeate stream from the gas mixture A–B. This mechanism applies to separating gas mixtures with very different molecular sizes such as H_2 and CO_2, H_2 and hydrocarbons, etc. Some common gas kinetic diameters are given in **Table 2**. Size sieving basically performs in micro-porous membrane.

http://dx.doi.org/10.5772/65723

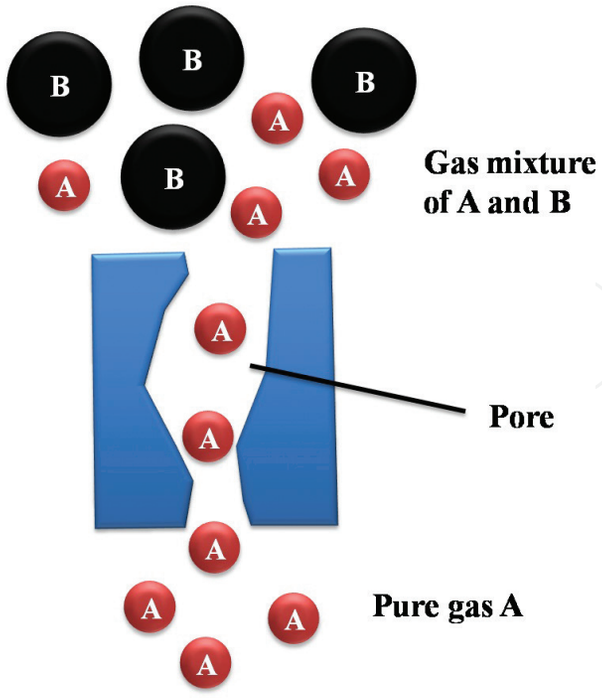


Figure 5. Size sieving separation mechanism.

2.3.2. Surface diffusion

When the membrane material has higher affinity to one particular component than the other, this affinitive component is preferentially adsorbed on the membrane surface and then the adsorbed gas molecules move along the pore surface to the permeate side until desorbing to the permeate gas. Since the membrane is occupied by the highly adsorbable component, the less adsorbed component has lower probability to access the pore, which results in a much lower permeability. In such a way, the more adsorbable gas is separated from the gas mixture (**Figure 6**). This type of mechanism is generally used to separate adsorbing gas with non-adsorbing gas such as CO_2 with He, CO_2 with H_2. Surface diffusion generally acts in micro- and meso-porous membranes.

Gas	σ (nm)
He	0.26
H_2	0.289
CO_2	0.33
Ar	0.341
O_2	0.346
N_2	0.364
CH_4	0.38

Table 2. The kinetic diameter of different gases.

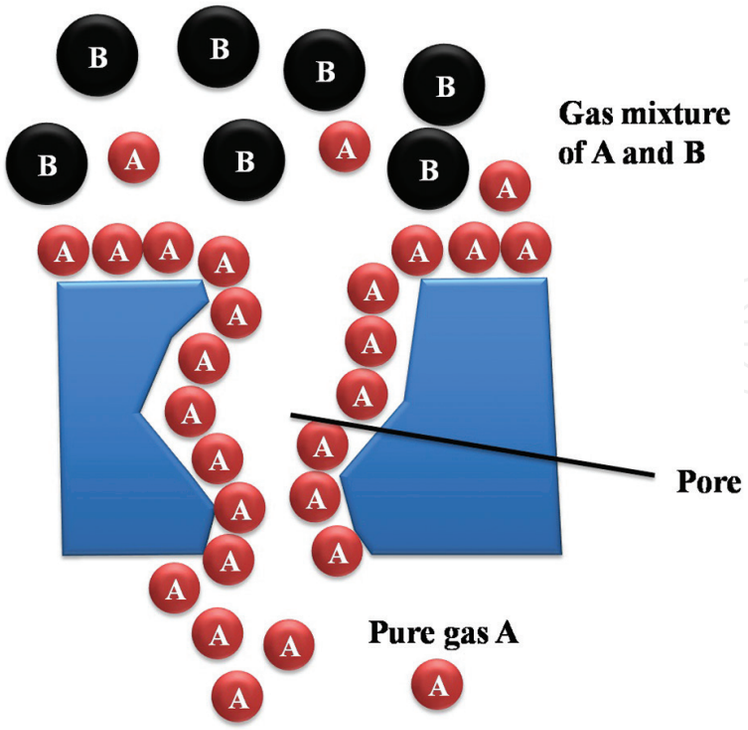


Figure 6. Surface diffusion separation mechanism.

2.3.3. Solution diffusion

Unlike membranes discussed above, dense membrane has no pore channel for gas transportation. However, it follows solution diffusion model. The process of gas separation using dense membranes occurs in a three-step process, which is similar to surface diffusion. The dense membrane has no pore to accommodate gas molecules, however, it can solve specific gas component. As shown in **Figure 7**, due to the difference in solubility or absorbability in the membrane material, gas A solves or absorbs in the membrane after they contact at the feed interface, while gas B still remains as gas phase at the interface. The second step is the solved A component diffusing across the membrane driven by the concentration gradient from feed interface to the permeate interface. Finally, component A desorbs from the permeate interface under a low pressure. This is a common mass transfer mechanism in polymeric membrane.

2.3.4. Facilitated transport

The solution-diffusion process is often constrained by low permeate flux rates due to a combination of low solubility and/or low diffusivity. In contrast, facilitated transport that delivers the target component by a carrier can increase the permeate flow rate. As demonstrated in **Figure 8**, the gas A and carrier C form a temporary product A–C that is from a reversible chemical reaction. The product diffuses across the membrane under the concentration gradient of this product A–C instead of the concentration gradient of A. At the permeate interface, the reverse reaction takes place and A is liberated from this reverse

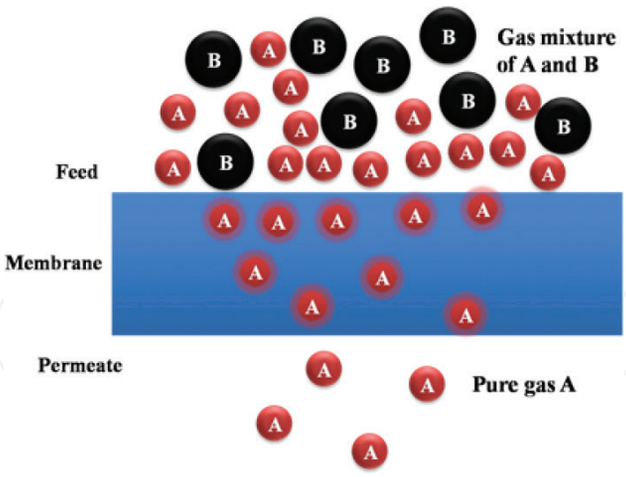


Figure 7. Solution diffusion separation mechanism.

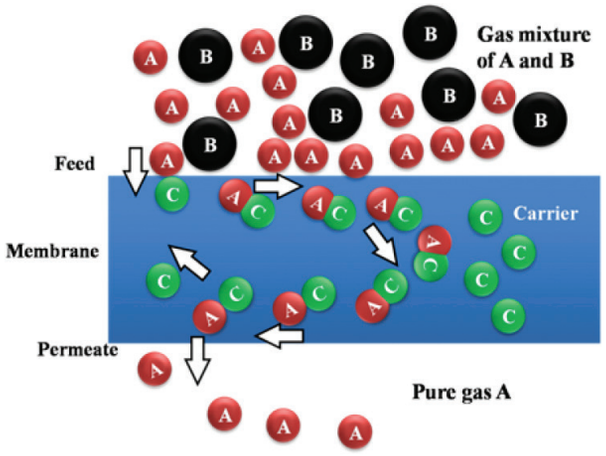


Figure 8. Facilitated transport separation mechanism.

reaction. A is released to the permeate stream and C diffuses back to the feed interface again to attach and deliver a new A. Facilitated transport mechanism normally exists in liquid membrane.

2.3.5. Ion transport

Ion transport is usually applied in air separation (O_2/N_2). As **Figure 9** shows, only oxygen gas molecule (O_2) can be converted into two oxygen ions ($2O^{2-}$) by the surface-exchange reaction on the feed interface. Nitrogen retains in the feed side. Oxygen ions are transported across by jumping between oxygen vacancies in the membrane lattice structure. At the permeate interface, electrons liberated as the oxygen ions recombine into oxygen molecules. To maintain electrical neutrality, there is a simultaneous electrons flux going back to the feed interface neutralizing the charge caused by oxygen flux.

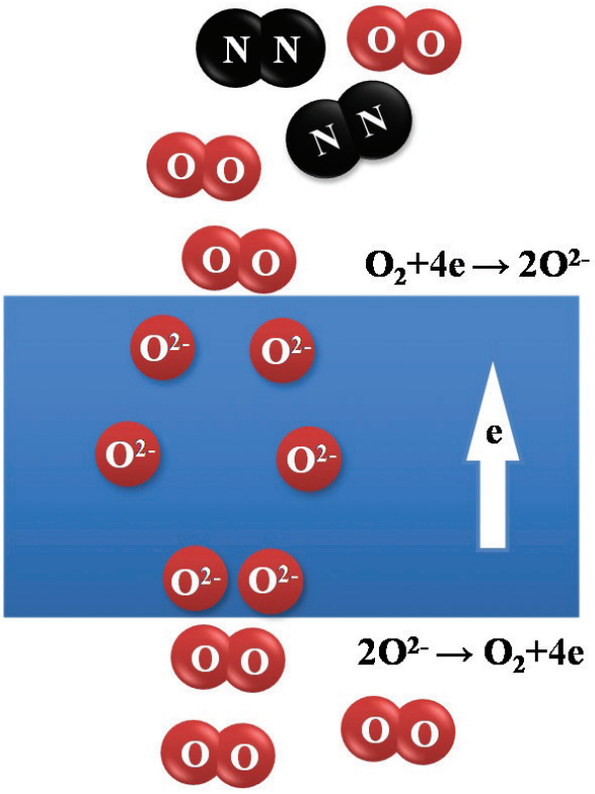


Figure 9. Ion transport separation mechanism.

3. Membranes for pre-combustion capture

Pre-combustion capture is a process that separates CO_2 from the other fuel gases before the gas combustion. First, it involves the processes of converting solid, liquid or gaseous fuels into a mixture of syngas (H_2 and CO) and CO_2 by coal gasification or steam reforming. Afterwards water-gas shift (WGS) reaction is conducted to reduce the content of CO, thus more H_2 and CO_2 are generated. Membrane separation is then applied to separate H_2 and CO_2. Upon compression, the CO_2 rich stream is transported to a storage or utilization site. Meanwhile, the nearly pure H_2 stream enters the combustion chamber for power generation that emits mainly water vapor in the exhaust.

Coming from the upstream gasification, reforming and WGS, the feed gas of pre-combustion CO_2 capture is hot with a temperature between 300 and 700°C. In addition, the pre-combustion separation can happen at high pressures up to 80 bar.

Pre-combustion membranes are basically classified into two categories: H_2-selective membrane and CO_2-selective membrane. The former favors H_2 permeation but retains CO_2 in the feed side, while the latter preferentially permeates CO_2.

In principle, metallic membrane is the ideal candidate for separating H_2/CO_2 due to the infinite selectivity. H_2 molecule dissociates as two H atoms at the membrane surface and then the

http://dx.doi.org/10.5772/65723

atomic H diffuses to the permeate side of the membrane driven by the partial pressure drop, which is followed by the association and desorption at the permeate interface. The permeate flux is given by

$$J_{H_2} = \frac{P_{H_2}}{L}\left(\sqrt{p_{feed}} - \sqrt{p_{permeate}}\right). \quad (1)$$

This mechanism is similar to solution diffusion and ion transport. The reason for the infinite selectivity of H_2 over CO_2 is that this dissociation-diffusion mechanism only applies to diatomic gases such as H_2 and CO_2 cannot permeate by the same mechanism. For ultrathin membrane, the rate-limiting step is the dissociation of hydrogen on the membrane surface and Pd material performs the best in hydrogen dissociation. Consequently, Pd membrane was intensively investigated in the past several decades. H_2 permeability through palladium membrane varies in the range between 10^{-7} and 10^{-8}mol s^{-1} m^{-1} $Pa^{-0.5}$ (**Table 3**). However, the permeability was not satisfactory for the industrial requirement yet. This is due to the slow permeation of H atom in the lattice of Pd, which is one order of magnitude lower than in other metals. In order to promote the permeability, a number of palladium-based alloys have been examined. A list of reported permeability data are summarized in **Table 4**. The alloy membranes dramatically improve the H_2 permeability by 2–3 orders of magnitude.

Still, a few barriers need to be overcome for the commercialization of palladium-based membrane. First, the cost of palladium is around 18,000 US$/Ounce (in June 2016), which is 150 times more expensive than silica membrane. Second, the H_2 permeation driving force is not from pressure; instead, it is from the root square of pressure (Eq. (1)). Therefore, the effect of compressing feed gas is not as significant as in other permeation mechanisms. In

Membrane	Permeability (mol s^{-1} m^{-1} $Pa^{-0.5}$)	Temperature (°C)	Reference
Pd	9×10^{-9}	227	[3]
Pd on sliver disk	1.47×10^{-7}	407	[4]
Pd disk	1.08×10^{-7}	300	[5]
Pd disk	1.06×10^{-7}	350	[6]
Pd disk from Pd sheet	7.25×10^{-7}	400	[7]
Pd on Vycor support	3.10×10^{-7}	350	[8]
Pd on Nickel	2.00×10^{-12}	200	[9]
Pd on Vycor support	1.18×10^{-7}	500	[10]
Pd on γ alumina	1.47×10^{-7}	480	[11]
Pd on alumina	6.27×10^{-8}	300	[12]
Pd on alumina	3.75×10^{-8}	400	[13]

Table 3. Hydrogen permeability through palladium membrane.

Membrane	Permeability (mol s^{-1} m^{-1} $Pa^{-0.5}$)	Temperature (°C)	Reference
$Pd_{59}Cu_{41}$	1.59×10^{-7}	400	[6]
$Pd_{60}Cu_{40}$	1.57×10^{-7}	350	[5]
$Pd_{60}Cu_{40}$	1.78×10^{-7}	400	[5]
$Pd_{94}Cu_{6}$	3.65×10^{-8}	400	[14]
$Pd_{50}Ni_{50}$	7.00×10^{-6}	450	[15]
$Pd_{69}Ag_{30}Ru_{1}$	1.03×10^{-6}	400	[13]
$Pd_{70}Ag_{30}$	2.35×10^{-7}	400	[13]
$Pd_{77}Ag_{23}$	1.35×10^{-7}	350	[16]
$Pd_{77}Ag_{23}$	5.00×10^{-5}	450	[17]
$Pd_{93}Ag_{7}$	7.25×10^{-8}	400	[14]

Table 4. Hydrogen permeability through palladium-based alloy.

addition, at temperatures lower than 300°C, hydrogen embrittlement causes catastrophic failure. Furthermore, the contaminations such as CO, NH_3 and sulfur compounds inhibit H_2 permeation through palladium membrane. Currently, palladium membrane separation still remains in small laboratory scale.

Besides metal membrane, inorganic membrane also plays an important role in separating H_2/CO_2 at elevated temperatures. The separation by inorganic membrane is generally achieved by the molecular size sieving effect. Carbon molecular sieve membrane has demonstrated in pilot scale to separate H_2 from refiner gas streams in the early 1990s. The disadvantage of carbon membrane is that it is only feasible in non-oxidizing condition. Another type of inorganic membrane is alumina membrane. However, the majority pore size is not in the range of micropore and cannot separate gas by the size sieving mechanism. Due to the large pore size, the selectivity of alumina membrane is fairly low.

Silica membrane shows great commercial potential for separating H_2 and CO_2. It is one of the most abundant materials on the planet, thus the cost is significantly reduced. Also the good thermal and chemical stability makes it possible to work in long term without frequent replacement or maintenance. The pore diameter could be controlled around 0.3 nm by proper coating-calcining process, which is the ideal size for separating H_2 (σ = 0.26 nm) and CO_2 (σ = 0.33 nm). The performance of some reported silica membranes is summarized in **Table 5**. Due to the difficulty in measuring the membrane thickness on porous substrate, permeability of H_2 divided by thickness is lumped together as permeance.

The H_2 permeance of silica membrane could reach up to the order of 10^{-6} mol s^{-1} m^{-2} Pa^{-1}, which strongly suggests that silica membrane is competitive in pre-combustion capture. However, exposure to high concentration water vapor leads to a decline in performance of silica membrane. Such a steady decay over long time can cause the H_2 permeance decrement by an order of magnitude. This still inhibits the commercialization of silica membrane.

Membrane	Permeance (mol s^{-1} m^{-2} Pa^{-1})	H_2/CO_2 selectivity	Temperature (°C)	Reference
Silica (Si400)	2.01×10^{-6}	7	200	[18]
Silica (hydrophobic)	1.51×10^{-6}	6	200	[19]
Silica on zirconia	1.34×10^{-6}	4	300	[20]
Silica	1.34×10^{-6}	8	300	[20]
Silica (Si600)	5.02×10^{-7}	200	[18]	
Silica (hydrophilic)	6.70×10^{-9}	11	200	[19]
Silica with Co	5.00×10^{-9}	1000	250	[21]
Silica	1.80×10^{-8}	15–80	150	[22]
Silica with Co&Pd	6.00×10^{-6}	200	500	[23]
Silica (ES40)	1.01×10^{-6}	12	450	[24]
AKP-30 tubular silica	1.8×10^{-6}	3.5	200	[25]
Silica with C6 surfactant	1.5×10^{-6}	6	200	[19]
Silica without C6 surfactant	7.0×10^{-9}	10	200	[19]

Table 5. H_2/CO_2 separation performance by silica-based membrane.

As a nonporous membrane, polymeric membrane permeates gases via the solution-diffusion mechanism. Permeability is a function of gas diffusivity and solubility. The hydrogen molecules diffuse faster than other gases due to the small molecular size. However, the lower solubility of hydrogen within the polymeric membrane reduces its permeability. For H_2-selective polymeric membranes, the permeability is limited by the low solubility of H_2. There is a wide range of polymeric membranes available for H_2 separation from CO_2. The performance of some polymeric membranes is shown in **Table 6**. High permeabilities are observed for polyimides such as 6FDA-durene. Higher selectivities are reported for polybenzimidazole and poly(vinyl chloride), but H_2 permeability is compromised.

Membrane	Permeability (mol s^{-1} m^{-2} Pa^{-1})	H_2/CO_2 selectivity	Temperature (°C)	Reference
6FDA-Durene	1.89×10^{-9}	1	35	[26]
Polybenzimidazole	3.15×10^{-12}	45	35	[27]
Poly(vinyl chloride)	5.36×10^{-12}	11	35	[28]
Poly(vinyl chloride)	6.30×10^{-12}	11	30	[29]
Polybenzimidazole	2.89×10^{-13}	9	20	[30]
	4.10×10^{-11}	20	270	
	3.41×10^{-11}	3	300	

Table 6. H_2/CO_2 separation performance by polymeric membrane.

The only shortcoming of polymeric membranes is the poor thermal stability at operating temperatures more than 100°C. Only polybenzimidazole was examined at the temperature range (300–700°C) for syngas purification. For polybenzimidazole membrane, the greatest performance in H_2 permeability and H_2/CO_2 selectivity is observed between 200 and 270°C. This peak performance can be related to the increasing diffusivity of the smaller H_2 molecule as temperature increases. More importantly, the performance of polymeric membranes depends on its stability in the environment of the real process. For example, exposure to gases such as CO_2, water vapor and H_2S may results in plasticization and mechanical fouling.

Due to the good thermal and hydrothermal stability, zeolite membranes were also viewed as another possible candidate for separation of H_2 and CO_2. Zeolite has ordered pore structure. If the pore channel size is proper, efficient size sieving could be achieved. Despite the relative simple concept, only a few types of zeolite are workable since this molecular sieve mechanism requires perfect membranes. This remains a challenge for zeolite membranes. The performance of a number of reported H_2/CO_2 separation using zeolite membranes is summarized in **Table 7**. In general, neither H_2 permeance nor H_2/CO_2 selectivity can exceed ~10^6 mol s^{-1} m^{-2} Pa^{-1} and ~50 to meet the industrial demands.

Metal organic framework (MOF) membrane has been an emerging candidate for H_2/CO_2 separation. In MOF materials, metal or metal oxide cluster cations are interconnected by organic anions. The coordination polymers form flexible frameworks, therefore such MOFs are called 'soft porous crystals'. **Table 8** summarizes the H_2 permeance and H_2/CO_2 selectivity using

Membrane	Permeance[a] (mol s^{-1} m^{-2} Pa^{-1}) or Permeability[b] (mol s^{-1} m^{-1} Pa^{-1})	H_2/CO_2 selectivity	Temperature (°C)	Reference
MFI	2.82×10^{-7}[a]	42.6	500	[31]
MFI	1.50×10^{-7}[a]	5	200	[32]
MFI template free	1.50×10^{-8}[a]	3	500	[33]
DDR	5.00×10^{-8}[a]	5	500	[34]
DDR by CVD	2.24×10^{-8}[a]	5.9	500	[35]
Zeolite-A	9.45×10^{-10}[a]	10	35	[36]
MFI	1.76×10^{-9}[a]	18	450	[37]
$AlPO_4$-5 Zeolite	3.15×10^{-9}[a]	24	35	[38]
ZSM-5	5.68×10^{-8}[a]		110	[39]
ZIF-69	6.60×10^{-8}[a]	1.8	25	[40]
13X with PI	6.93×10^{-11}[b]	2.8	25	[41]

[a]Permeance.
[b]Permeability.

Table 7. H_2/CO_2 separation performance by zeolite membranes.

Membrane	Permeance (mol s^{-1} m^{-2} Pa^{-1})	H_2/CO_2 selectivity	Temperature (°C)	Reference
MOF5	2.80×10^{-6}	4.3	25	[42]
MOF5	4.40×10^{-7}	4.4	25	[43]
MOF5	8.00×10^{-7}	3.5	25	[44]
Ni-MOF-74	1.27×10^{-5}	9.1	25	[45]
NH_2-MIL-53 (Al)	1.98×10^{-6}	30.9	25	[46]
MIL-53	5.00×10^{-7}	4	25	[47]
ZIF-7	7.40×10^{-7}	6.7	200	[48]
ZIF-7	4.55×10^{-7}	13	220	[49]
ZIF-7	4.57×10^{-6}	9.6	25	[50]
ZIF-7	3.05×10^{-6}	18.3	170	[50]
ZIF-8	5.00×10^{-8}	3.5	25	[51]
ZIF-8	1.80×10^{-7}	3	25	[52]
ZIF-8	2.66×10^{-5}	8.8	100	[53]
ZIF-22	2.00×10^{-7}	7.2	25	[54]
ZIF-90	2.95×10^{-7}	16.9	225	[55]
ZIF-95	1.90×10^{-6}	25.7	52	[56]
JUC-150	1.83×10^{-7}	38.7	25	[57]
HKUST-1	1.10×10^{-6}	5.5	190	[58]
MMOF	2.00×10^{-9}	5	190	[59]

Table 8. H_2/CO_2 separation performance by MOF membranes.

different MOF membranes. Despite relatively moderate permselectivity, attractively high permeances are observed. The operating temperature for MOF membranes is normally lower than the pre-combustion temperatures, owing to organic ligands. The synthesis of MOF membranes is relatively sophisticated so that the cost has to be notably reduced toward commercialization. There is still a long way for MOF membranes to fulfill the demands of industrial applications.

Unlike H_2-selective membranes, CO_2-selective membranes preferentially permeate CO_2 and thus they also enable the separation of CO_2 and H_2. Separating CO_2 from H_2 can only be realized through surface diffusion or solution diffusion driven by the difference in adsorb-ability or solubility between the gases. However, retaining the small molecules of H_2 but permeating the larger CO_2 is really challenging. To maximize the difference of adsorption or solution between the two gases, the temperature is required to be low, however, low temperatures are not favored by pre-combustion processes. From this point of view, CO_2-selective membranes are much less applicable than H_2-selective ones.

4. Membranes for post-combustion capture

Another situation where we need to separate CO_2 is after the fuel combustion. The exhaust gas (flue gas) mainly contains CO_2, H_2O and N_2. H_2O vapor is easy to be removed by condensation. More efforts are required to separate CO_2 and N_2 prior to further treatments such as compression. Unlike pre-combustion capture, post-combustion capture separates CO_2/N_2 at moderate temperatures and ambient atmosphere pressure. Such operating conditions seem less severe than those of pre-combustion processes. As a result, post-combustion capture has encountered much less difficulties and is therefore rather closer to practical application. The major challenge for post-combustion capture is the low CO_2 volumetric fraction in flue gas, that is, ~15%, which results in a low driving force of CO_2 permeation.

The separation of CO_2/N_2 mainly rely on surface diffusion and solution diffusion, which is driven by the difference in adsorb-ability and solubility between the gases. The good thing is that, compared to N_2, $CO_2$is more likely to be favored by majority of the membrane materials via adsorption or absorption. Furthermore, the diameter of CO_2 is slightly smaller than that of N_2, which also enhances the diffusion of CO_2 (see **Table 2**). Therefore, for post-combustion capture, CO_2-selective membranes are generally used.

To capture CO_2 from flue gas, a membrane should satisfy a few requirements such as high CO_2 permeability, high CO_2/N_2 selectivity, high thermal and chemical stability and acceptable costs. So far, polymer-based membranes are the only commercially viable type for CO_2 removal from flue gas. The membrane materials include cellulose acetate, polymides, polysulfone and polycarbonates. **Table 9** shows the performance of several such membranes.

Membrane	Permeance[a] (mol s^{-1} m^{-2} Pa^{-1}) or Permeability[b] (mol s^{-1} m^{-1} Pa^{-1})	CO_2/N_2 selectivity	Temperature (°C)	Reference
Cellulose acetate	2.48×10^{-7a}	40.17	Not reported	[60]
Polymides-TMeCat	6.30×10^{-10b}	25	30	[61]
Polymides-TMMPD	1.89×10^{-9b}	17.1	Not reported	[62]
Polymides-IMDDM	6.17×10^{-10b}	18.1	Not reported	[62]
Polysulfone-HFPSF-o-HBTMS	3.31×10^{-10b}	18.6	35	[63]
Polysulfone-HFPSF-TMS	3.47×10^{-10b}	18	35	[64]
PolysulfoneTMPSF-HBTMS	2.27×10^{-10b}	21.4	35	[65]
Polycarbonates-TMHFPC	3.50×10^{-10b}	15	35	[66]
Polycarbonates-FBPC	4.76×10^{-11b}	25.5	35	[67]

[a]Permeance.
[b]Permeability.

Table 9. CO_2/N_2 separation performance by polymer-based membranes.

Selectivity larger than 20 was observed for all the polymer-based membranes with decent permeability. The high solubility of CO_2 in polymers ensures sufficient CO_2/N_2 selectivity. Furthermore, polymers with a high fractional free volume present excellent gas transport properties.

Mixed-matrix membrane is a new option to enhance the properties of polymeric membranes. The microstructure consists of an inorganic material in the form of micro- or nanoparticles in discrete phase incorporated into a continuous polymeric matrix. The addition of inorganic materials in a polymer matrix offers improved thermal and mechanical properties for aggressive environments and stabilizes the polymer membranes against the changes in chemical and physical environments. Carbon molecular sieves membranes also show interesting performance for CO_2 separation applications. Polyimide is the most used precursor for carbon membranes. Carbon membranes improved gas transport properties for light gases (molecular size smaller than 4.0–4.5Å) with thermal and chemical stability. The major disadvantages of mixed-matrix and carbon membranes that hinder their commercialization include brittleness and the high cost that is 1–3 orders of magnitude greater than polymeric membranes.

5. Membranes for oxy-fuel combustion

In oxy-fuel combustion, oxygen is supplied for combustion instead of air. This avoids the presence of nitrogen in the exhaust gas, the major issue to be solved by post-combustion CO_2 capture technologies. With the use of pure oxygen for the combustion, the major composition of the flue gases is CO_2, water vapor, other impurities such as SO_2. Water vapor can be easily condensed and SO_2 can be removed by conventional desulphurization methods. The remained CO_2-rich gases (80–98 vol.% CO_2 depending on fuel used) can be compressed, transported and stored. This process is technically feasible but consumes large amounts of oxygen coming from an energy intensive air separation (O_2/N_2) unit.

The O_2/N_2separation follows the ion transport mechanism as depicted in **Figure 9** for air separation membrane. Oxygen molecules are converted to oxygen ions at the surface of the membrane and transported through the membrane by an applied electric voltage or oxygen partial pressure difference; these ions are reverted back to oxygen molecules after passing through the membrane. These membranes are O_2-selective in principle. Generally, fluorite-based and perovskite-based membranes are used to deliver oxygen through this mechanism.

Air separation is mostly carried out at atmosphere and meanwhile the permeate side connects to high speed sweep gas or vacuum. So, for convenience, the membrane performance is generally described as permeate flux instead of permeance. **Table 10** shows a list of oxygen permeation flux for the fluorite membranes. The oxygen permeation flux of fluorite-based membranes ranges from 10^{-4} to 10^{-6} mol s^{-1} m^{-2} between 650 and 1527°C. The highest oxygen flux was observed for $Bi_{1.5}Y_{0.3}Sm_{0.2}O_3$ compounds.

Membrane	O_2 flux (mol s^{-1} m^{-2})	Thickness (mm)	Temperature (°C)	Reference
$Bi_{0.75}Y_{0.5}Cu_{0.75}O_3$	2.80×10^{-5}–1.06×10^{-4}	2	650–850	[68]
$Bi_{1.5}Y_{0.3}Sm_{0.2}O_3$	4.40×10^{-3}–6.36×10^{-3}	1.2	825–875	[69]
$Ce_{0.8}Pr_{0.2}O_{2-\delta}$	1.33×10^{-4}–3.35×10^{-4}	1	850–950	[70]
$(ZrO_2)_{0.85}(CaO)_{0.15}$	1.70×10^{-4}	1	870	[71]
$[(ZrO_2)_{0.8}(CeO_2)_{0.2}]_{0.9}(CaO)_{0.1}$	1.36×10^{-6}–9.44×10^{-5}	2	1127–1527	[72]

Table 10. Oxygen permeation flux data for fluorite membranes.

Membrane	O_2 flux (mol s^{-1} m^{-2})	Thickness (mm)	Temperature (°C)	Reference
$BaBi_{0.4}Co_{0.2}Fe_{0.4}O_{3-\delta}$	3.064×10^{-3}–5.985×10^{-3}	1.5	800–925	[73]
$BaCo_{0.4}Fe_{0.5}Zr_{0.1}O_{3-\delta}$	1.908×10^{-3}–6.813×10^{-3}	1	700–950	[74]
$CaTi_{0.8}Fe_{0.2}O_{3-\delta}$	7.976×10^{-5}–2.185×10^{-4}	1	800–1000	[75]
$Gd_{0.6}Sr_{0.4}CoO_{3-\delta}$	1.179×10^{-2}	1.5	820	[76]
$LaCo_{0.8}Fe_{0.2}O_{3-\delta}$	1.786×10^{-4}	1.5	860	[76]
$La_{0.6}Sr_{0.4}Co_{0.8}Cu_{0.2}O_{3-\delta}$	1.417×10^{-2}	1.5	860	[76]
$SrCo_{0.8}Fe_{0.2}O_{3-\delta}$	2.485×10^{-2}	1	870	[77]

Table 11. Oxygen permeation flux data for perovskite membranes.

Performance of perovskite membranes are displayed in **Table 11**. Oxygen permeation flux with the magnitude of 10^{-2}–10^{-5} mol s^{-1} m^{-2} between 700 and 100°C was reported. The overall oxygen flux through perovskite membrane is superior to fluorite membrane. $SrCo_{0.8}Fe_{0.2}O_{3-\delta}$ exhibits the best oxygen flux.

In spite of a great number of works that attempt to efficiently separate air using membrane, the membrane technology for oxy-fuel combustion is still at its early stage of development. Compared to the conventional cryogenic air separation technique, the high temperature requirement and the resulting high costs of air separation membrane are unfavorable for commercialization. Some other issues such as high temperature sealing, chemical and mechanical stability and so on also need to be addressed prior to practical application. At present, there has not been any full scale oxy-fuel membrane project reported.

6. Summary of membranes applied in CCS

The aforementioned membranes are compared in **Table 12**. Their application situation, advantages and disadvantages are summarized accordingly.

Membrane type	Application	Advantages	Disadvantages
Metal membrane	Pre-combustion	Infinite H_2/CO_2 selectivity	High cost; poisoning; low driving force
Carbon membrane	Pre-combustion	Size sieving effect; high H_2/CO_2 selectivity	High cost; susceptible to oxygen; brittleness
Alumina membrane	Pre-combustion	Low cost; chemical and physical stability	Low H_2/CO_2 selectivity
Zeolite membrane	Pre-combustion and post-combustion	Low cost; chemical and physical stability	Low H_2/CO_2 selectivity
MOF membrane	Pre-combustion and post-combustion	Large pore volume and surface area	High cost
Silica membrane	Pre-combustion	Proper pore size; low cost; high thermal stability	Poor hydrothermal stability
Polymeric membrane	Post-combustion	Low cost; high CO_2/N_2 selectivity	Low chemical and physical stability; too thick
Fluorite membrane	Oxy-fuel combustion	High O_2/N_2 selectivity	Energy intensive; hard to seal
Perovskite membrane	Oxy-fuel combustion	High O_2/N_2 selectivity	Energy intensive; hard to seal; poisoning

Table 12. The summarization of membranes in CCS.

7. Membrane mass transfer theory

Membrane separation technique has been intensified with the growing needs for CCS. The major two targets of membrane are chasing high permeability and selectivity. The understanding of gas transport through membrane is of great importance in providing the guidance of membrane material design and synthesis improvement.

For all mass transfer problems, a general form is always expressed as a coefficient multiplied by a driving force as

$$J = C \cdot f. \tag{2}$$

where J is the mass transfer flux, C is the general transfer coefficient and f is the general driving force. The driving force can be the gradient of pressure, concentration, chemical potential or even electrical potential depending on the mass transfer mechanism. The coefficient can be permeability, diffusivity or other term depending on the term of driving force. For membrane mass transfer, the pressure difference and permeate flux are generally determined from experimental measurements, so the most common form in membrane industry is

$$J = \left(\frac{P}{l}\right) \cdot \Delta p. \tag{3}$$

Membrane thickness l is lumped together with permeability P into a term called permeance $\left(\frac{P}{l}\right)$, which is a convenient form of addressing permeation due to the difficulty in

measuring the exact thickness of thin films. Generally, membrane films interpenetrate into the pores of the interlayer or substrate (interlayer-free membrane). Hence, the thickness is not homogenous.

7.1. Viscous flow model

When the pore size is large, the gas molecule-molecule collision is relatively dominant than gas molecule-wall collision. That means the mean free path is far less than the pore size

$$\frac{\lambda}{d} \ll 1, \tag{4}$$

where λ is the mean free path and d is the diameter of the pore.

In such situation, viscosity plays an important role in the mass transfer and the permeate flux across the membrane is described by viscous flow model:

$$J = -\frac{\varepsilon_p}{\tau_T}\frac{r_p^2}{8\eta}\frac{p}{RT}\frac{\mathrm{d}p}{\mathrm{d}z}, \tag{5}$$

where η is the viscosity, R is the gas constant, T is the temperature, p is the pressure, ε_p is the porosity of the pore, τ_T is the tortuosity of the pore and r_p is the pore radius. Viscosity increases with temperature for gases. From Eq. (5), it should be noted that if the transportation is in the viscous regime, the flux is a decreasing function of temperature. Although the viscosity is different from gas to gas, gas mixtures share a singular viscosity value when they are well mixed due to the intensive intermolecular collision. Therefore, there is no selectivity for all gases in the viscous regime even if they have different viscosities.

7.2. Knudsen diffusion model

When the pore size is reduced down to the scale much smaller than mean free path, the molecular-wall collision is more dominating than intermolecular collision. In this situation, the viscosity is not playing a role for the gas transportation. Instead, the pore geometry and gas molecule velocity influence more significantly in the mass transfer. This type of transport is called Knudsen diffusion. If the molecule to wall collisions is dominant over intermolecular collision, the Knudsen number must be much higher than 1.

$$Kn = \frac{\lambda}{d} \gg 1, \tag{6}$$

where Kn is called Knudsen number. The permeate flux is described by the Knudsen diffusion model

$$J = -\frac{2}{3}\frac{\varepsilon_p r_p}{\tau_T}\sqrt{\frac{8}{\pi \mathrm{R}T\mathrm{M}}}\frac{\mathrm{d}p}{\mathrm{d}z} = -\frac{2}{3}\frac{\varepsilon_p r_p}{\tau_T}\sqrt{\frac{8}{\pi \mathrm{R}T\mathrm{M}}}\frac{\Delta p}{l}, \tag{7}$$

where M is the molecular weight.

Based on Eq. (3) the permeance of Knudsen diffusion is

$$\left(\frac{P}{l}\right) = -\frac{2}{3}\frac{\varepsilon_p r_p}{\tau_T l}\sqrt{\frac{8}{\pi \mathrm{R}T\mathrm{M}}}\,. \tag{8}$$

For the same pore at a fixed temperature, the permeate flux is determined by the molar weight and in principle, the selectivity is the root square of the reciprocal of molar weights. However, due to the limited selectivity, Knudsen diffusion is rarely used in practice for separating real gas mixtures.

7.3. Surface diffusion model

For ultra-micro-porous (d_p < 5Å) material, the Lennard-Jones (L-J) potential from atoms, which forms the pore wall starts to overlap inside the pore. Consequently, there is a very deep potential well around the wall and the distance from wall to the well is around the scale of gas molecule diameter. In this situation, the gas molecule's motion is significantly affected by the potential fields. Since the intrinsic nature of gas is seeking for lower potential, thus adsorption preferentially takes place around the pore wall due to the existence of the potential well. As such, the model is called surface diffusion. A brief introduction has been given in Section 2.3.2. of this chapter, but here a more analytical and mathematical description of surface diffusion will be provided.

The original expression of mass transfer across the membrane is given by

$$J = -qD\frac{1}{RT}\frac{\mathrm{d}\mu}{\mathrm{d}z}, \tag{9}$$

where q is the molar concentration of gas in the pore, D is the diffusivity, μ is the chemical potential and z is the space coordinate in the membrane thickness direction.

Assuming equilibrium between the membrane surface concentration and the bulk gas phase, the following relationship for the chemical potential is applicable

$$\mu_0 = \mu + RT\ln p, \tag{10}$$

where p is the absolute pressure.

Using Eq. (10), Eq. (9) is converted to

$$J = -D\frac{\mathrm{d}\ln p}{\mathrm{d}\ln q}\frac{\mathrm{d}q}{\mathrm{d}z} = -D\Gamma\frac{\mathrm{d}q}{\mathrm{d}z}. \tag{11}$$

$\Gamma = \dfrac{\mathrm{d}\ln p}{\mathrm{d}\ln q}$ is defined as thermodynamic factor. In micro-porous material, the adsorbed gas concentration generally follows Langmuir isotherm,

$$q = q_{\mathrm{sat}}\frac{b\mathrm{p}}{1+b\mathrm{p}}, \tag{12}$$

where b is Langmuir equilibrium constant. Bring Eq. (12) to Eq. (11) gives

$$J = -q_{\mathrm{sat}}D\frac{1}{1-\theta}\frac{\mathrm{d}\theta}{\mathrm{d}z}, \tag{13}$$

where $\theta = \frac{q}{q_{sat}}$ is called occupancy. Thermal dynamic factor $\Gamma = \frac{1}{1-\theta}$ is derived from Langmuir isotherm. Surface diffusion is often applied in separating gas mixtures, which has very different adsorption capacity in the same material.

However, with elevated temperature, the adsorption is getting weaker and Langmuir isotherm is approaching to Henry's law.

$$q = Kp, \tag{14}$$

where K is Henry's constant. Bring Eq. (14) to Eq. (11), we get Fick's first law

$$J = -D\frac{\mathrm{d}q}{\mathrm{d}z}. \tag{15}$$

Diffusivity D is a function of temperature. The temperature dependence usually obeys an Arrhenius relation

$$D = D_0 \exp\left(-\frac{E_d}{RT}\right), \tag{16}$$

where D_0 is a pre-exponential coefficient depending on the average distance, the frequency and average velocity of gas jump and E_d is diffusion activation energy. Henry's constant is a function of temperature according to a van't Hoff relation:

$$K = K_0 \exp\left(\frac{Q}{RT}\right), \tag{17}$$

where K_0 is a pre-exponential coefficient, Q is the heat of adsorption.

Eqs. (14)–(17) can be combined as

$$J = -D_0 K_0 \exp\left(-\frac{E_d - Q}{RT}\right)\frac{\mathrm{d}p}{\mathrm{d}z} = -D_0 K_0 \exp\left(-\frac{E_a}{RT}\right)\frac{\mathrm{d}p}{\mathrm{d}z}. \tag{18}$$

E_a is called apparent activation energy, which is defined as

$$E_a = E_d - Q. \tag{19}$$

Apparent activation energy determines whether the permeate flux is an increasing function to temperature or not, so this type of diffusion is called activated transport.

Assuming a uniform pressure gradient, Eq. (18) is simplified to

$$J = -D_0 K_0 \exp\left(-\frac{E_a}{RT}\right)\frac{\Delta p}{l}. \tag{20}$$

The permeance $\left(\frac{P}{l}\right)$ is the coefficient between flux and pressure drop according to Eq. (3)

$$\left(\frac{P}{l}\right) = \frac{D_0 K_0}{l}\exp\left(-\frac{E_a}{RT}\right). \tag{21}$$

http://dx.doi.org/10.5772/65723

Activated transport is generally used to separate gas mixtures, which has different sign of apparent activation energy and the separation performance will be enhanced at elevated temperatures.

7.4. Gas translation diffusion model

If the pore size is further reduced to the molecular level, there is no potential well inside the pore. Instead, the positive potential overlaps, which forms a potential barrier. Only the gas molecules, which have kinetic energy higher than the potential barrier, are possible to make a successful jump to complete permeation. This model is called gas translation diffusion. The permeate flux of gas translation follows Fick's first law as derived in Eq. (15) with the difference in diffusion coefficient term.

$$D_{\mathrm{GT}} = \frac{\lambda}{Z_{\mathrm{n}}}\sqrt{\frac{8RT}{\pi M}}\exp^{\left(-\frac{E_{\mathrm{GT}}}{RT}\right)}, \tag{22}$$

where λ is the jump length, Z_{n} is the number of available jump directions and E_{GT} is the potential barrier. By considering ideal gas law

$$p = cRT. \tag{23}$$

Gas translation permeance should rewrite as

$$\left(\frac{P}{l}\right) = \frac{\lambda}{Z_{\mathrm{n}}}\sqrt{\frac{8}{\pi \mathrm{MRT}}}\exp^{\left(\frac{E_{\mathrm{GT}}}{RT}\right)}. \tag{24}$$

7.5. Oscillator model

If we assume the pore is a cylinder, the gas molecules are hopping in the pore cylinder from entrance to the exit. The gas molecule trajectory looks like oscillating on the pore cross section. The gas travels with speed between collisions and loses all the momentum when colliding on the wall. This model is a more recent development in mass transfer theory by Bhatia et al. [78, 79].

From Newton's law,

$$\left\langle \mathrm{v_z} \right\rangle = \frac{D}{k_B T} f = \frac{f}{m}\langle \tau \rangle, \tag{25}$$

the gas diffusivity in the pore is derived

$$D = \frac{k_B T}{m}\langle \tau \rangle, \tag{26}$$

where $\langle v_z \rangle$ is the average velocity in the permeation direction, k_B the Boltzmann constant, f the force, m the molecule mass and $\langle \tau \rangle$ the average hopping time. The hopping time of each molecule depends on the pore potential distribution, its radial coordinate and momentum

$$\tau(r, p_r, p_\theta) = 2m\int_{\mathrm{r_{c0}(r,P_r,P_\theta)}}^{\mathrm{r_{c1}(r,P_r,P_\theta)}} \frac{\mathrm{d}\, r'}{p_r\left(r', r, p_r, p_\theta\right)}. \tag{27}$$

$p_r(r', r, p_r, p_\theta)$ is the radial momentum at r' of a molecule, which had radial momentum p_r at r. $r_{c1}(r, p_r, p_\theta)$ and $r_{c0}(r, p_r, p_\theta)$ are the r' solution of radial momentum $p_r(r', r, p_r, p_\theta) = 0$. The radial momentum is derived from the conservation of total energy or Hamiltonian

$$E_t(r, p_r, p_\theta) = \phi(r) + \frac{p_r^2}{2m} + \frac{p_\theta^2}{2m r^2}, \tag{28}$$

where $\phi(r)$ is the radial L-J potential, which could be derived from pore structure and gas property. The force in radial direction is the partial derivative of total energy with respect to r

$$\frac{\mathrm{d}\, p_r}{\mathrm{d}t} = -\frac{\partial E_t}{\partial r}. \tag{29}$$

Combining Eqs. (28) and (29) gives the radial momentum

$$p_r(r', r, p_r, p_\theta) = \left\{2m\left[\phi(r) - \phi(r')\right] + p_r^2(r) + \frac{p_\theta}{r^2}\left(1 - \frac{r^2}{r'^2}\right)\right\}^{1/2}. \tag{30}$$

Considering a canonical distribution for p_r and p_θ, we have

$$\psi(r, p_r, p_\theta) = \psi_0 \exp\left[-\frac{1}{RT}\left(\phi(r) + \frac{p_r^2}{2m} + \frac{p_\theta^2}{2m r^2}\right)\right]. \tag{31}$$

The diffusion coefficient expression is obtained from Eqs. (26), (30) and (31)

$$D(r_p, T) = \frac{2}{\pi m \int_0^\infty r\, e^{-\frac{\phi(r)}{RT}}\,\mathrm{d}r} \int_0^\infty e^{-\frac{\phi(r)}{RT}}\,\mathrm{d}r \int_0^\infty e^{-\frac{p_r^2}{2mRT}}\,\mathrm{d}\,p_r \int_0^\infty e^{-\frac{p_\theta^2}{2mr^2RT}}\,\mathrm{d}\,p_\theta \int_{r_{c0}(r,p_r,p_\theta)}^{r_{c1}(r,p_r,p_\theta)} \frac{\mathrm{d}\,r'}{p_r(r', r, p_r, p_\theta)}. \tag{32}$$

Oscillator model is a pure theoretical and analytical approach without any empirical or semi-empirical factors. It takes account adsorption effect and applies to all pore sizes, pressure and temperatures.

Besides the mass transfer models introduced above, there are some other methods to study the membrane gas transport from a theoretical perspective. Monte Carlo and molecular dynamics are also major techniques to investigate the micropore mass transfer. Because this chapter focused on membrane CCS technology rather than transport phenomena, other sophisticated theories are not demonstrated here.

8. Current status of membrane application

8.1. Membranes for pre-combustion

The membrane separation for pre-combustion is not a mature technology so far. There has not been industry-scale membrane system. However, a few pilot scale pre-combustion membrane systems have demonstrated the potential of extending the system to enlarged scale.

Eltron Research & Development Inc. developed a pilot-scale pre-combustion membrane with 100 kg day^{-1} H_2 production from 2005. They employed alloy membrane to separate H_2 accord-

ing to Sieverts' Law. This project successfully improved membrane-based integrated gasification combined cycle (IGCC) flow sheets, achieving carbon capture greater than 95%.

Another pilot-scale pre-combustion membrane set-up was constructed by Worcester Polytechnic Institute's (WPI) in 2010. More than 566 L H_2 was produced per day. Stable H_2 fluxes were achieved in actual syngas atmospheres at 450°C for more than 470 h under 12 bar pressure difference. The implement MembraGuardTM (T3's technology) inhibited surface poisoning by hydrogen sulfide (H_2S) and H_2 permeation showed good stability for more than 250 h.

8.2. Membranes for post-combustion

Membrane separation for post-combustion is a relatively mature technique. In 1995, the largest membrane-based natural gas processing plant in the world was built in Kadanwari, Pakistan. Cellulose acetate membrane was applied in this project to separate CO_2. The Kadanwari system is a two-stage unit designed to treat 25×10^5 m^3 h^{-1} of feed gas at 90 bar. The CO_2 content is reduced from 12% to less than 3%.

After Kadanwari plant, the Qadirpur plant started in the same year and the processing capacity exceeded Kadanwari plant with 31×10^5 m^3 h^{-1} of feed gas at 59 bar. The CO_2 content is reduced from 6.5 to 2%. The Qadirpur plant was upgraded to 64×10^5 m^3 h^{-1} of feed gas in 2003.

8.3. Membranes for oxy-fuel combustion

Air separation membrane is still in its early stage. In view of the high energy requirement of ion transport mechanism, air separation membrane can hardly challenge the traditional cryogenic air separation for large scale product.

Air products, which have been developing ion transport membrane technology since 1988 and the DOE (US Department of Energy) are collecting data from a pilot plant near Baltimore in Maryland, with the capacity of 5 tons of oxygen per day. This facility will lead to the next step of designing and building a larger membrane air separation unit (150 tons oxygen per day).

9. Techno-economic of membrane

The conventional CO_2 capture process is absorption (with ammines). Amine-based absorption is the most common technology. However, the corrosion, degradation and high regeneration energy of amine significantly increase the electricity cost. Substantial technological improvements and alternative technologies are highly needed to lower the CO_2 capture cost.

The economic indicator CO_2 avoided ($/ton) is an established term for measuring and comparing different CO_2 capture strategies such as absorption, adsorption, cryogenic separation and membrane separation. It is the additional cost of establishing and running a CO_2 capture facility for an industrial plant or power plant compared to the respective plant without CO_2 capture. The CO_2 avoided is expressed as:

$$CO_2 \text{ avoided} = \frac{\text{LCOE(capture)} - \text{LCOE(ref.)}}{CO_2 \text{ emission(ref.)} - CO_2 \text{ emission(capture)}}, \quad (33)$$

where ref. and capture mean the reference plant without capture and the respective plant with CO_2 capture facility. LCOE is the levelized cost of electricity which is expressed as:

$$\text{LCOE} = \frac{\text{sum of cost over lifetime}}{\text{sum of electrical energy produced over lifetime}}. \quad (34)$$

A brief techno-economic comparison was made between two power plants using conventional amine scrubbers in and a power plant using polymer membrane (**Table 13**). The estimates are subject to uncertainty because we cannot accurately predict all input parameters such as fuel price, operational and maintenance cost. The aim of the comparison is not to give absolute costs, but to illustrate indicatively that the costs per ton CO_2 avoided. The overall comparison indicates that the case employing membrane separation results in slightly lower LCOE and CO_2 avoided than traditional amine-based solvent scrubbing. Although this cannot judge the membrane economical advantage, the comparison at least indicates that membrane separation is competitive to the amine-based solvent scrubbing. However, significant efforts are still required to improve the membrane properties so as to achieve higher stability, permeate purity and recovery.

Organization		**Carnegie Mellon University**	**Electric Power Research Institute**	**Membrane Technology and Research, Inc**
CCS technology		Amine-based	Amine-based	Membrane-based
Location		USA	USA	USA
Coal type		Bitcoal	Bitcoal	Illinois#6
Plant size (MW)		575	600	580
Designed CO_2 capture rate (%)		90	85	90
CO_2 emission (kg/MWh)	Reference	811	836	760
	Capture	107	126	87
Net power output (MW)	Reference	528	600	550
	Capture	493	550	461
Net plant efficiency (LHV, %)	Reference	41.4	40	41.4
	Capture	31.5	29.1	34.4
Efficiency penalty (%)		9.9	10.9	7
Capital costs ($/kW)	Reference	1696	2104	1727
	Capture	2759	3516	2627
LCOE ($/MWh)	Reference	62	77	62
	Capture	104	127	93
CO_2 avoided ($/ton)		58	71	46

Table 13. Techno-economic comparisons between amine-based CO_2 removal and membrane separation.

http://dx.doi.org/10.5772/65723

Author details

Guozhao Ji and Ming Zhao*

*Address all correspondence to: ming.zhao@tsinghua.edu.cn

School of Environment, Tsinghua University, Beijing, China

References

[1] Brinker, C. J.; Scherer, G. W., Sol-gel science. *Material Science* **1989**,*6* (1), 475–495.

[2] Khatib, S. J.; Oyama, S. T.; Souza, K. R. D., et al., Chapter 2–Review of silica membranes for hydrogen separation prepared by chemical vapor deposition. *Journal of Membrane Science & Technology* **2011**,*14* (25), 25–60.

[3] Holleck, G. L., Diffusion and solubility of hydrogen in palladium and palladium–silver alloys. *The Journal of Physical Chemistry* **1970**,*74* (3), 503–511.

[4] Govind, R.; Atnoor, D., Development of a composite palladium membrane for selective hydrogen separation at high temperature. *Industrial & Engineering Chemistry Research* **1991**,*30* (3), 591–594.

[5] Mckinley D L. Method for hydrogen separation and purification: US, US 3439474 A[P]. 1969.

[6] Gade, S. K.; Thoen, P. M.; Way, J. D., Unsupported palladium alloy foil membranes fabricated by electroless plating. *Journal of Membrane Science* **2008**,*316* (1–2), 112–118.

[7] Morreale, B. D.; Ciocco, M. V.; Enick, R. M., et al., The permeability of hydrogen in bulk palladium at elevated temperatures and pressures. *Journal of Membrane Science* **2003**,*212* (1–2), 87–97.

[8] Altinisik, O.; Dogan, M.; Dogu, G., Preparation and characterization of palladium-plated porous glass for hydrogen enrichment. *Catalysis Today* **2005**,*105* (3–4), 641–646.

[9] Zhang, Y.; Gwak, J.; Murakoshi, Y., et al., Hydrogen permeation characteristics of thin Pd membrane prepared by microfabrication technology. *Journal of Membrane Science* **2006**,*277* (1), 203–209.

[10] Uemiya, S.; Sato, N.; Ando, H., et al., The water gas shift reaction assisted by a palladium membrane reactor. *Industrial & Engineering Chemistry Research* **2002**,*30* (3), 585–589.

[11] Zhang, X.; Xiong, G.; Yang, W., A modified electroless plating technique for thin dense palladium composite membranes with enhanced stability. *Journal of Membrane Science* **2008**,*314* (1–2), 226–237.

[12] Itoh, N.; Akiha, T.; Sato, T., Preparation of thin palladium composite membrane tube by a CVD technique and its hydrogen permselectivity. *Catalysis Today* **2005**,*104* (2), 231–237.

[13] Wang, L.; Yoshiie, R.; Uemiya, S., Fabrication of novel Pd–Ag–Ru/Al_2O_3 ternary alloy composite membrane with remarkably enhanced H2 permeability. *Journal of Membrane Science* **2007**,*306* (1), 1–7.

[14] Uemiya, S.; Sato, N.; Ando, H., et al., Separation of hydrogen through palladium thin film supported on a porous glass tube. *Journal of Membrane Science* **1991**,*56* (3), 303–313.

[15] Se, N.; Kh, L., A study on the palladium/nickel composite membrane by vacuum electrodeposition. *Journal of Membrane Science* **2000**,*170* (1), 91–99.

[16] Abate, S.; Genovese, C.; Perathoner, S., et al., Performances and stability of a Pd-based supported thin film membrane prepared by EPD with a novel seeding procedure. Part 1–Behaviour in H_2:N_2 mixtures. *Catalysis Today* **2009**,*145* (1–2), 63–71.

[17] Tong, H. D.; Gielens, F. C.; Gardeniers, J. G. E., et al., Microfabricated palladium-silver alloy membranes and their application in hydrogen separation. *Industrial & Engineering Chemistry Research* **2004**,*43* (15), 4182–4187.

[18] de Vos, R. M.; Verweij, H., Improved performance of silica membranes for gas separation. *Journal of Membrane Science* **1998**,*143* (1–2), 37–51.

[19] Giessler, S.; Jordan, L.; Costa, J. C. D. D., et al., Performance of hydrophobic and hydrophilic silica membrane reactors for the water gas shift reaction. *Separation and Purification Technology* **2003**,*32* (1–3), 255–264.

[20] Yoshioka, T.; Nakanishi, E.; Tsuru, T., et al., Experimental studies of gas permeation through microporous silica membranes. *AIChE Journal* **2001**,*47* (9), 2052–2063.

[21] Battersby, S.; Tasaki, T.; Smart, S., et al., Performance of cobalt silica membranes in gas mixture separation. *Journal of Membrane Science* **2009**,*329* (1–2), 91–98.

[22] Diniz da Costa, J. C.; Lu, G. Q.; Rudolph, V., et al., Novel molecular sieve silica (MSS) membranes: characterisation and permeation of single-step and two-step sol–gel membranes. *Journal of Membrane Science* **2002**,*198* (1), 9–21.

[23] Ballinger, B.; Motuzas, J.; Smart, S., et al., Palladium cobalt binary doping of molecular sieving silica membranes. *Journal of Membrane Science* **2014**,*451*, 185–191.

[24] Miller, C. R.; Wang, D. K.; Smart, S., et al., Reversible redox effect on gas permeation of cobalt doped ethoxy polysiloxane (ES40) membranes. *Scientific Reports* **2013**,*3*, 1–6.

[25] Richard, V.; Favre, E.; Tondeur, D., et al., Experimental study of hydrogen, carbon dioxide and nitrogen permeation through a microporous silica membrane. *Chemical Engineering Journal* **2001**,*84* (3), 593–598.

[26] Chung, T. S.; Lu, S.; Pei, S. T., Surface modification of polyimide membranes by diamines for H_2 and CO_2 separation. *Macromolecular Rapid Communications* **2006**,*27* (13), 998–1003.

[27] Choi, S.; Coronas, J.; Lai, Z., et al., Fabrication and gas separation properties of polybenzimidazole (PBI)/nanoporous silicates hybrid membranes. *Journal of Membrane Science* **2008**,*316* (1–2), 145–152.

[28] Tikhomirov, B. P.; Hopfenberg, H. B.; Stannett, V., et al., Permeation, diffusion and solution of gases and water vapor in unplasticized poly(vinylchloride). *Die Makromolekulare Chemie* **1968**,*118* (1), 177–188.

[29] Robeson, L. M., Polymer membranes for gas separation. *Current Opinion in Solid State & Materials Science* **1999**,*4* (6), 549–552.

[30] Pesiri, D. R.; Jorgensen, B.; Dye, R. C., Thermal optimization of polybenzimidazole meniscus membranes for the separation of hydrogen, methane and carbon dioxide. *Journal of Membrane Science* **2003**,*218* (1–2), 11–18.

[31] Zhang, Y.; Wu, Z.; Zhou, H., et al., Hydrogen-selective zeolite membrane reactor for low temperature water gas shift reaction. *Chemical Engineering Journal* **2012**,*197* (14), 314–321.

[32] Burggraaf, A. J.; Vroon, Z. A. E. P.; Keizer, K., et al., Permeation of single gases in thin zeolite MFI membranes. *Journal of Membrane Science* **1998**,*144* (144), 77–86.

[33] Kanezashi, M.; O'Brien, J.; Lin, Y. S., Template-free synthesis of MFI-type zeolite membranes: permeation characteristics and thermal stability improvement of membrane structure. *Journal of Membrane Science* **2006**,*286* (1–2), 213–222.

[34] Tomita, T.; Nakayama, K.; Sakai, H., Gas separation characteristics of DDR type zeolite membrane. *Microporous and Mesoporous Materials* **2004**,*68* (1), 71–75.

[35] Kanezashi, M.; O'Brien-Abraham, J.; Lin, Y. S., et al., Gas permeation through DDR-type zeolite membranes at high temperatures. *AIChE Journal* **2008**,*54* (6), 1478–1486.

[36] Aoki, K.; Kusakabe, K.; Morooka, S., Gas permeation properties of A-type zeolite membrane formed on porous substrate by hydrothermal synthesis. *Journal of Membrane Science* **1998**,*141* (2), 197–205.

[37] Gu, X.; Tang, Z.; Dong, J., On-stream modification of MFI zeolite membranes for enhancing hydrogen separation at high temperature. *Microporous and Mesoporous Materials* **2008**,*111* (1), 441–448.

[38] Guan, G.; Tanaka, T.; Kusakabe, K., et al., Characterization of AlPO4-type molecular sieving membranes formed on a porous α-alumina tube. *Journal of Membrane Science* **2003**,*214* (2), 191–198.

[39] Richter, H.; Voigt, I.; Fischer, G., et al., Preparation of zeolite membranes on the inner surface of ceramic tubes and capillaries. *Separation and Purification Technology* **2003**,*32* (1), 133–138.

[40] Su, J.; Qian, Y.; Teo, J. F., et al., Cellulose acetate nanofiltration hollow fiber membranes for forward osmosis processes. *Journal of Membrane Science* **2010**,*355* (1–2), 36–44.

[41] Chaidou, C. I.; Pantoleontos, G.; Koutsonikolas, D. E., et al., Gas separation properties of polyimide-zeolite mixed matrix membranes. *Separation Science and Technology* **2012**,*47* (7), 950–962.

[42] Cao, F.; Zhang, C.; Xiao, Y., et al., Helium recovery by a Cu-BTC metal–organic-framework membrane. *Industrial & Engineering Chemistry Research* **2012**,*51* (34), 11274–11278.

[43] Zhao, Z.; Ma, X.; Li, Z., et al., Synthesis, characterization and gas transport properties of MOF-5 membranes. *Journal of Membrane Science* **2011**,*382* (1–2), 82–90.

[44] Yoo, Y.; Lai, Z.; Jeong, H. K., Fabrication of MOF-5 membranes using microwave-induced rapid seeding and solvothermal secondary growth. *Microporous and Mesoporous Materials* **2009**,*123* (1–3), 100–106.

[45] Lee, D. J.; Li, Q.; Kim, H., et al., Preparation of Ni-MOF-74 membrane for CO_2 separation by layer-by-layer seeding technique. *Microporous and Mesoporous Materials* **2012**,*163* (1), 169–177.

[46] Zhang, F.; Zou, X.; Gao, X., et al., Hydrogen selective NH_2-MIL-53(Al) MOF membranes with high permeability. *Advanced Functional Materials* **2012**,*22* (17), 3583–3590.

[47] Hu, Y.; Dong, X.; Nan, J., et al., Metal-organic framework membranes fabricated via reactive seeding. *Chemical Communications* **2010**,*47* (2), 737–739.

[48] Li, Y. S.; Liang, F. Y.; Bux, H., et al., Molecular sieve membrane: supported metal–organic framework with high hydrogen selectivity. *Angewandte Chemie International Edition* **2010**,*49* (3), 548–551.

[49] Li, Y.; Liang, F.; Bux, H., et al., Zeolitic imidazolate framework ZIF-7 based molecular sieve membrane for hydrogen separation. *Journal of Membrane Science* **2010**,*354* (1), 48–54.

[50] Melgar, V. M. A.; Kwon, H. T.; Kim, J., Direct spraying approach for synthesis of ZIF-7 membranes by electrospray deposition. *Journal of Membrane Science* **2014**,*459* (2), 190–196.

[51] Bux, H.; Liang, F.; Li, Y., et al., Zeolitic imidazolate framework membrane with molecular sieving properties by microwave-assisted solvothermal synthesis. *Journal of the American Chemical Society* **2009**,*131* (44), 16000–16001.

[52] Mccarthy, M. C.; Varelaguerrero, V.; Barnett, G. V., et al., Synthesis of zeolitic imidazolate framework films and membranes with controlled microstructures. *Langmuir* **2010**,*26* (26), 14636–14641.

[53] Huang, A.; Liu, Q.; Wang, N., Highly hydrogen permselective ZIF-8 membranes supported on polydopamine functionalized macroporous stainless-steel-nets. *Journal of Materials Chemistry A* **2014**,*2* (22), 8246–8251.

[54] Huang, A.; Bux, H.; Steinbach, F., et al., Molecular-sieve membrane with hydrogen permselectivity: ZIF-22 in LTA topology prepared with 3-aminopropyltriethoxysilane as covalent linker. *Angewandte Chemie International Edition* **2010**,*49* (29), 4958–4961.

[55] Huang, A.; Wang, N.; Kong, C., et al., Organosilica-functionalized zeolitic imidazolate framework ZIF-90 membrane with high gas-separation performance. *Angewandte Chemie* **2012**,*124* (42), 10703–10707.

[56] Huang, A.; Chen, Y.; Wang, N., et al., A highly permeable and selective zeolitic imidazolate framework ZIF-95 membrane for H(2)/CO(2) separation. *Chemical Communications* **2012**,*48* (89), 10981–10983.

[57] Kang, Z.; Xue, M.; Fan, L., et al., Highly selective sieving of small gas molecules by using an ultra-microporous metal-organic framework membrane. *Energy & Environmental Science* **2014**,*7* (12), 4053–4060.

[58] Guerrero, V. V.; Yoo, Y.; Mccarthy, M. C., et al., HKUST-1 membranes on porous supports using secondary growth. *Journal of Materials Chemistry* **2010**,*20* (19), 3938–3943.

[59] Ranjan, R.; Tsapatsis, M., Microporous metal organic framework membrane on porous support using the seeded growth method. *Chemistry of Materials* **2009**,*21* (20), 4920–4924.

[60] Ahmad, A. L.; Jawad, Z. A.; Low, S. C., et al., A cellulose acetate/multi-walled carbon nanotube mixed matrix membrane for CO_2/N_2 separation. *Journal of Membrane Science* **2014**,*451* (1), 55–66.

[61] Majdi Al-Masri; Detlev Fritsch; Kricheldorf Hans R., New polyimides for gas separation. 2. Polyimides derived from substituted catechol bis(etherphthalic anhydride)s. *Macromolecules* **2000**,*33* (19), 7127–7135.

[62] Abajo, J. D.; Campa, J. G. D. L.; Lozano, A. E., Designing aromatic polyamides and polyimides for gas separation membranes. *Macromolecular Symposia* **2003**,*199* (1), 293–306.

[63] Dai, Y.; Guiver M. D.; Robertson G. P., et al., Enhancement in the gas permeabilities of novel polysulfones with pendant 4-trimethylsilyl-α-hydroxylbenzyl substituents. *Macromolecules* **2003**,*36* (18), 6807–6816.

[64] Dai, Y.; Guiver, M. D.; Robertson, G. P., et al., Preparation and characterization of polysulfones containing both hexafluoroisopropylidene and trimethylsilyl groups as gas separation membrane materials. *Macromolecules* **2004**,*37* (4), 1403–1410.

[65] Dai, Y.; Guiver, M. D.; Robertson, G. P., et al., Modified polysulfones 5: synthesis and characterization of tetramethyl polysulfones containing trimethylsilyl groups and their gas transport properties. *Polymer* **2002**,*43* (20), 5369–5378.

[66] Hellums, M. W.; Koros, W. J.; Husk, G. R., et al., Fluorinated polycarbonates for gas separation applications. *Journal of Membrane Science* **1989**,*46* (1), 93–112.

[67] Aguilar-Vega, M.; Paul, D., Gas transport properties of polycarbonates and polysulfones with aromatic substitutions on the bisphenol connector group. *Journal of Polymer Science, Part B: Polymer Physics* **1993**,*31* (11), 1599–1610.

[68] Nigara, Y.; Mizusaki, J.; Ishigame, M., Measurement of oxygen permeability in CeO_2 doped CSZ. *Solid State Ionics* **1995**,*79*, 208–211.

[69] Akin, F. T.; Lin, Y. S., Selective oxidation of ethane to ethylene in a dense tubular membrane reactor. *Journal of Membrane Science* **2002**,*209* (2), 457–467.

[70] Fagg, D.; Marozau, I.; Shaula, A., et al., Oxygen permeability, thermal expansion and mixed conductivity of GdxCe$_{0.8-x}$ Pr$_{0.2}$O$_{2-\delta}$, x = 0, 0.15, 0.2. *Journal of Solid State Chemistry* **2006**,*179* (11), 3347–3356.

[71] Teraoka, Y.; Zhang, H.-M.; Furukawa, S., et al., Oxygen permeation through perovskite-type oxides. *Chemistry Letters* **1985**,*14* (11), 1743–1746.

[72] Nigara, Y.; Mizusaki, J.; Ishigame, M., Proceedings of the 20th commemorative symposium on solid state ionics in Japan measurement of oxygen permeability in CeO_2 doped CSZ. *Solid State Ionics* **1995**,*79*, 208–211.

[73] Shao, Z.; Xiong, G.; Cong, Y., et al., Synthesis and oxygen permeation study of novel perovskite-type BaBi$_x$ Co$_{0.2}$ Fe$_{0.8-x}$ O$_{3-\delta}$ ceramic membranes. *Journal of Membrane Science* **2000**,*164* (1–2), 167–176.

[74] Tong, J.; Yang, W.; Zhu, B., et al., Investigation of ideal zirconium-doped perovskite-type ceramic membrane materials for oxygen separation. *Journal of Membrane Science* **2002**,*203* (1–2), 175–189.

[75] Iwahara, H.; Esaka, T.; Mangahara, T., Mixed conduction and oxygen permeation in the substituted oxides for $CaTiO_3$. *Journal of Applied Electrochemistry* **1988**,*18* (18), 173–177.

[76] Teraoka, Y.; Nobunaga, T.; Yamazoe, N., Effect of cation substitution on the oxygen semipermeability of perovskite-type oxides. *Chemistry Letters* **1988**,*3* (3), 503–506.

[77] Teraoka, Y.; Zhang, H. M.; Furukawa, S., et al., Oxygen permeation through perovskite-type oxides. *Chemistry Letters* **1985**,*11* (11), 1743–1746.

[78] Jepps, O. G.; Bhatia, S. K.; Searles, D. J., Wall mediated transport in confined spaces: exact theory for low density. *Physical Review Letters* **2003**,*91* (12), 126102.

[79] Bhatia, S. K.; Jepps, O.; Nicholson, D., Tractable molecular theory of transport of Lennard-Jones fluids in nanopores. *The Journal of Chemical Physics* **2004**,*120* (9), 4472–4485.